

1 A Global Ozone Profile Climatology for Satellite Retrieval
2 Algorithms Based on Aura MLS Measurements and the
3 MERRA-2 GMI Simulation
4
5

6 Jerald R. Ziemke^{1,2}, Gordon J. Labow³, Natalya A. Kramarova¹, Richard D. McPeters¹, Pawan
7 K. Bhartia¹, Luke D. Oman¹, Stacey M. Frith³, David P. Haffner³
8

9 ¹NASA Goddard Space Flight Center, Greenbelt, Maryland, USA

10 ²Morgan State University, Baltimore, Maryland, USA

11 ³SSAI, Lanham, Maryland, USA
12

13 **Abstract.** A new atmospheric ozone profile climatology has been constructed by combining
14 [daytime](#) ozone profiles from the Aura Microwave Limb Sounder (MLS) and Modern-Era
15 Retrospective Analysis for Research Applications version 2 (MERRA2) Global Modeling
16 Initiative (GMI) model simulation (M2GMI). The MLS and M2GMI ozone profiles are merged
17 between 13 and 17 km (~159 and 88 hPa) with MLS used for stratospheric and GMI for
18 primarily tropospheric levels. The time record for profiles from MLS and GMI is August 2004-
19 December 2016. The derived seasonal climatology consists of monthly zonal-mean ozone
20 profiles in 5-degree latitude bands from 90°S-90°N covering altitudes (in Z* log-pressure
21 altitude) from zero to 80 km in 1 km increments. This climatology can be used as a priori
22 information in satellite ozone retrievals, in atmospheric radiative transfer studies, and as a
23 baseline to compare with other measured or model-simulated ozone. The MLS/GMI seasonal
24 climatology shows a number of improvements compared to previous ozone profile climatologies
25 based on MLS and ozonesonde measurements. These improvements are attributed mostly to
26 continuous daily global coverage of GMI tropospheric ozone compared to sparse regional
27 measurements from sondes. ~~Only daytime measurements for MLS are used in the MLS/GMI~~
28 ~~climatology compared to the previous MLS/sonde climatology that averaged MLS day and night~~
29 ~~measurements together; the daytime only measurements are important for applications involving~~

30 ~~the upper stratosphere and lower mesosphere where the ozone diurnal cycle is large.~~ In addition
31 to the seasonal climatology, we also derive an additive climatology to account for inter-annual
32 variability in stratospheric zonal-mean ozone profiles which is based on a rotated empirical
33 orthogonal function (REOF) analysis of Aura MLS ozone profiles. This REOF climatology
34 starts in 1970 and captures most of the inter-annual variability in global stratospheric ozone
35 including Quasi-Biennial Oscillation (QBO) signatures.

37 1. Introduction.

38
39 McPeters and Labow (2012) (hereafter, ML) and Labow et al. (2015) combined ozone profile
40 data from ozonesondes and the Aura Microwave Limb Sounder (MLS) (Livesey et al., 2011) to
41 use as climatological a priori information for satellite retrievals of ozone. These ozone profile
42 climatologies were constructed by merging ozonesondes in the troposphere with satellite ozone
43 in the stratosphere/mesosphere. For the ML climatology the stratosphere/mesosphere portion of
44 the climatological ozone profiles was based on averaging MLS daytime and nighttime limb
45 measurements. The mix of daytime and nighttime measurements led to smearing of the ozone
46 diurnal cycle in the upper stratosphere and lower mesosphere.

Formatted: Not Highlight

Formatted: Not Highlight

47
48 The limited amount and sparse spatial coverage of ozonesonde data has led us to now use the
49 NASA Goddard Earth Observing System (GEOS) Global Modeling Initiative (GMI) model as a
50 substitute for the ozonesonde data in the lower atmosphere. The GMI model uses Modern-Era
51 Retrospective Analysis for Research Applications version 2 (MERRA2) meteorology. We refer
52 to this as the MERRA2 GMI (hereafter M2GMI) model.

53
54 We have generated a new ozone profile zonal-mean seasonal climatology (MLS/GMI) based on
55 combining MLS v4.2 and M2GMI ozone profiles which represents an improvement from our
56 previous sonde-satellite ozone climatologies including ML. The earlier climatologies were
57 binned in 10-degree latitude bands due mostly to the limited coverage of sondes. In contrast, the
58 new MLS/GMI ozone profile climatology has been binned to 5° latitude bands by taking
59 advantage of better spatial and temporal coverage of the model output. This new climatology
60 also extends to 80 km in altitude compared to 65 km in the previous climatologies. The new

61 MLS/GMI ozone profile climatology is provided for both volume mixing ratio (units ppmv) and
62 vertical column concentration (Dobson Units (DU) km⁻¹).

63
64 We also generated a new inter-annual ozone profile climatology ~~that is~~-based on MLS ozone,
65 SBUV total ozone, and rawinsonde wind data using a rotated empirical orthogonal function
66 (REOF) method. This REOF inter-annual climatology, just like the MLS/GMI seasonal
67 climatology includes monthly-zonal mean profile ozone concentration (units DU km⁻¹) within 5°
68 latitude bands and altitudes 0-80 km; however, the REOF climatology represents a long time-
69 dependent record beginning 1970 rather than a 12-month time record for the MLS/GMI
70 climatology.

71
72 The application of the MLS/GMI seasonal climatology by itself or together with ~~the~~ REOF
73 inter-annual climatology as a priori enables more accurate profile and column ozone retrievals,
74 including improvements for inter-calibrating and merging independent satellite ozone
75 measurements such as for the SBUV Merged Ozone Dataset (MOD) (Frith et al., 2014). The
76 REOF climatology has recently been used to improve the calibration of long-record ozone
77 measurements from ground Umlkehr instruments (I. Petropavlovskikh, personal communication,
78 2021) and from series of SBUV instruments. The REOF climatology has also recently been used
79 to improve SBUV ozone profile retrievals by adding inter-annual variability which nadir
80 instruments can not retrieve due to a coarse vertical resolution. These SBUV ozone profiles with
81 improved inter-annual variability can be used for long-record inter-annual variability of the
82 assimilated profile ozone records like one from the Goddard Modeling and Assimilation Office
83 (GMAO)-(K. Wargan, personal communication, 2021).

84
85 In the following sections we describe the data and GMI model output used in our analysis,
86 outline the methods used to construct the MLS/GMI seasonal climatology and REOF
87 climatology, and discuss the properties of the climatologies. We conclude with a summary of
88 our results. Additional details and figures not covered in the main text are included in a
89 Supplementary Material section.

91 **2. Ozone data and M2GMI model simulated ozone.**

92

93 **2.1. Aura MLS Ozone.**

94

95 The Microwave Limb Sounder (MLS) instrument onboard the Aura spacecraft makes ozone
96 profile measurements along the orbital track in both daytime and nighttime. Aura is in a sun
97 synchronous orbit, and therefore MLS has nearly complete latitude coverage each day between
98 82°S and 82°N, with local equatorial crossing times of approximately 1:45 pm for the ascending
99 sunlit portion of the orbit and 1:45 am for the nighttime descending node.

100

101 The MLS instrument is a thermal-emission microwave limb sounder that measures vertical
102 profiles of mesospheric, stratospheric, and upper tropospheric temperature, ozone, and several
103 other trace gases from limb scans made ahead of Aura about 7 minutes before the satellite
104 reaches the same point directly below. The MLS instrument primarily uses the 240 GHz
105 microwave band for v4.2 ozone retrievals which for recommended scientific applications extend
106 from 0.0215 hPa to 261 hPa on 38 pressure layers. Vertical spacing for these layers is about 1.3
107 km everywhere below 1 hPa and about 2.7 km at most altitudes above 1 hPa. By comparison,
108 the vertical resolution for the ozone retrievals is reported to be ~3 km extending from 261 hPa up
109 into the mesosphere. Further details regarding the MLS measurements are described by Livesey
110 et al. (2011). The time record for the MLS ozone used in our study was August 2004 –
111 December 2016. Given the high quality of MLS ozone in the low mesosphere we extend the
112 climatology to 80 km from 65 km where the ML climatology ended. We use only [MLS](#)
113 [measurements at ascending part of the orbit with a local equatorial crossing time at ~1:45 pm.](#)
114 [For most latitudes, that corresponds to](#) the daytime measurements ($SZA < 90^\circ$) from MLS in
115 [ozone profile climatology](#) since the daytime data is most appropriate for many passive UV/Vis
116 ozone remote sensing techniques that require daytime measurements. A number of studies of the
117 diurnal ozone variations in stratospheric and mesospheric ozone [Parrish et al., 2014; Frith et al.,
118 2020, and references therein] demonstrated sizeable diurnal ozone variations around 5-10 hPa.

119

120 **2.2. SBUV MOD total ozone record.**

121

122 We use MOD total column ozone measurements from the Solar Backscatter UltraViolet (SBUV)
123 v8.6 retrievals merged ozone dataset (MOD) as a proxy to reproduce time-dependent inter-
124 annual variability for the REOF climatology described in Section 4. The MOD total ozone
125 dataset (Frith et al., 2014) is comprised of a composite set of measurements from several SBUV
126 instruments. The first instrument was Nimbus-4 BUV launched in 1970, followed by the second
127 and improved version SBUV on Nimbus-7 launched in October 1978. Starting in 1989, seven
128 SBUV/2 instruments were launched beginning with NOAA-9, followed by NOAA 11, 14, 16,
129 17, 18, and 19. Currently~~Now~~ this record is extended with the Ozone Mapping and Profiler
130 Suite (OMPS) nadir-profiler (NP) on board the Suomi National Polar-orbiting Partnership
131 (SNPP) satellite. There are four follow-up OMPS instrumental suites as a part of JPSS program
132 (with JPSS-1/NOAA-20 already in operation) that will extend the SBUV-type ozone
133 observations in the next two decades. The SBUV instruments retrieve broad ozone profiles from
134 measurements of backscattered solar UV radiation which can be integrated to give total column
135 ozone. All MOD instrument measurements have been processed using the v8.6 retrieval
136 algorithm as described by McPeters et al. (2013) and Bhartia et al. (2013). In this study we use
137 monthly zonal-mean gridded total ozone extending from 90°S to 90°N at 5° latitudinal binning
138 (Frith, 2021, personal communication). The MOD total ozone record spans from January 1970
139 to December 2020 with some temporal gaps, including May 1976-October 1978 due to missing
140 Nimbus-4 BUV measurements.

141

142 **2.3. Ozonesonde measurements.**

143

144 We include balloon-launched ozonesonde measurements for comparison and validation of the
145 M2GMI simulated tropospheric ozone. The used ozonesonde database extends from 2004-2019
146 and includes measurements from the Southern Hemisphere ADditional OZonesondes
147 (SHADOZ) program (Thompson et al., 2017; Witte et al., 2017), the World Ozone and
148 Ultraviolet Data Center (WOUDC) (<https://woudc.org/>), and the Network for the Detection of
149 Atmospheric Composition Change (NDACC). (<http://www.ndsc.ncep.noaa.gov/>). The
150 ozonesondes provide daily ozone profile concentrations generally a few times per week as a
151 function of altitude; we include ozonesonde data from several dozen global sites. Most of the
152 sonde ozone profile measurements that we use are from Electrochemical Concentration Cell

153 ~~(ECC) instruments.~~ The ~~sonde~~ ozone profiles ~~we~~are integrated vertically each day from surface
154 to tropopause to derive tropospheric column ozone (TCO) measurements using the same
155 tropopause pressures as used for M2GMI TCO. Tropopause pressure for both sonde and GMI
156 TCO ~~measurements~~ was derived from National Centers for Environmental Prediction (NCEP)
157 re-analyses based on the World Meteorological Organization (WMO) 2K km⁻¹ temperature
158 lapse-rate definition. ~~Most all of the sonde ozone profile measurements that we use are from~~
159 ~~Electrochemical Concentration Cell (ECC) instruments.~~

160
161 In section 4 we describe construction of the REOF inter-annual ozone profile climatology that
162 includes monthly tropical Quasi-Biennial Oscillation (QBO) zonal winds ~~in its construction~~. The
163 tropical QBO zonal winds come from the Maldives (January 1970 - December 1975) and
164 Singapore (January 1976 - present) rawinsonde record (Univ. Berlin, [https://www.geo.fu-](https://www.geo.fu-berlin.de/met/)
165 [berlin.de/met/](https://www.geo.fu-berlin.de/met/)).

166 167 **2.4. MERRA-2 GMI simulated ozone.**

168
169 The M2GMI simulation is produced with the Goddard Earth Observing System (GEOS)
170 modeling framework (*Molod et al.*, 2015), using winds, temperature, and pressure from the
171 MERRA-2 reanalysis (*Gelaro et al.*, 2017). The configuration for this study is a dynamically
172 constrained replay (*Orbe et al.*, 2017) coupled to the Global Modeling Initiative's (GMI)
173 stratospheric and tropospheric chemical mechanism (*Duncan et al.*, 2007; *Oman et al.*, 2013;
174 *Nielsen et al.*, 2017). The simulation was run at ~0.5° horizontal resolution, on the cubed sphere,
175 and output on the same 0.625° longitude x 0.5° latitude grid as MERRA-2 from 1980-2016. We
176 refer to Strode et al. (2015, 2020) for details of the M2GMI model simulation. The daily
177 M2GMI ozone profiles were averaged monthly and re-gridded from the original resolution to
178 zonal means in 5° latitude bands; the original 72 layers of the simulated profile ozone were also
179 re-mapped to Z* altitudes with 1 km vertical spacing (section 3.2).

180 181 **2.4.1. Evaluation of M2GMI simulated tropospheric ozone.**

182

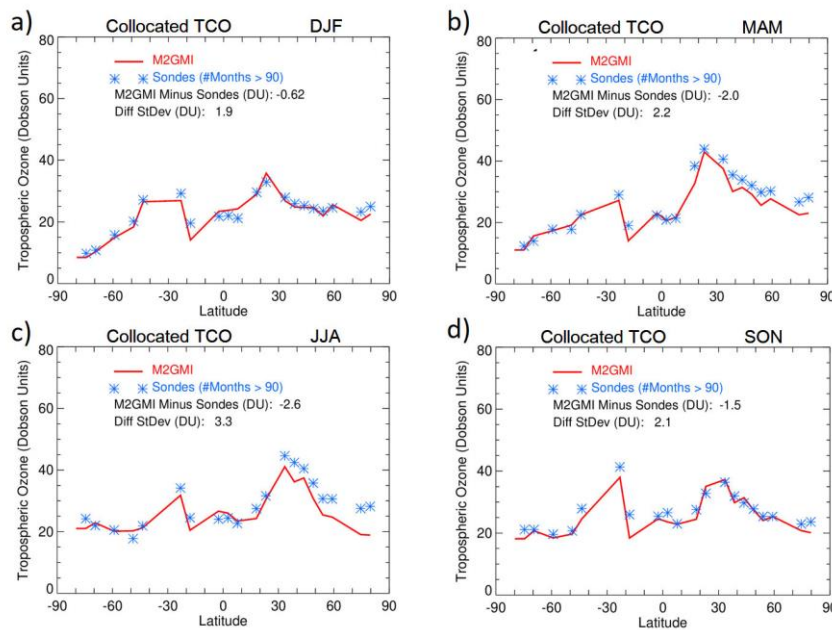
183 Ozone profiles generated by the M2GMI simulation have been extensively evaluated in a
184 number of studies. Stauffer et al. (2019) provides a detailed global analysis of M2GMI ozone
185 profiles using comparisons with ozonesondes. On average they found differences of about $\pm 5\%$
186 between M2GMI and sondes in the troposphere from 38 sonde stations from 69°S-79°N (their
187 Fig. 1). The largest differences were in the tropics where M2GMI was lower than sonde by up to
188 10-20% in low-mid troposphere, but in the tropical tropopause region M2GMI was higher than
189 sonde by 40-50%; the large percentage differences however can be due to relatively low mean
190 background ozone concentrations of only $\sim 1\text{-}2$ DU km^{-1} . Wargan et al. (2018) compared the
191 annual mean ozone mixing ratio anomalies for 1998-2016 between sondes and M2GMI at
192 several stations for 70 hPa, 100 hPa, and 200 hPa. Their comparisons show squared correlations
193 varying from 0.62 to 0.93 and they concluded that the M2GMI simulation well captures the
194 variability of tropospheric ozone including the UTLS region. Ziemke et al. (2014) provide
195 additional evaluation of M2GMI tropospheric ozone by comparing with ozonesondes, satellite,
196 and Global Modeling and Assimilation Office (GMAO) data assimilation; the M2GMI and sonde
197 daily comparisons from tropics to high latitudes in both hemispheres (their Figs. 2-7) showed
198 offsets and ~~difference~~ standard deviations of differences varying $\sim 0\text{-}2$ DU ($\sim 0\text{-}7\%$) and $4\text{-}7$ DU
199 ($\sim 15\text{-}23\%$), respectively. The M2GMI simulated ozone profiles have also been extensively
200 compared with Atmospheric Tomography Mission (ATom) aircraft flight measurements
201 (Bourgeois et al., 2020) for years 2015 and 2016 (Junhua Liu, personal communication, 2020).
202 The ATom in-flight measurements of ozone volume mixing ratio are found to compare closely
203 with M2GMI simulated ozone, generally within about $\pm 20\%$ along each of the mission flight
204 paths that included meandering ascent and descent between near surface and tropopause each
205 day.

206
207 Our study also includes evaluation of M2GMI simulated tropospheric ozone. Figure 1 compares
208 sonde and M2GMI Tropospheric Column Ozone (TCO) where the sonde and M2GMI
209 measurements have been space-time co-located at the sonde station sites and seasonally averaged
210 for 2004-2016. The collocation involved matching daily TCO from the sondes with M2GMI
211 daily TCO at $5^\circ \times 5^\circ$ gridded resolution interpolated to each sonde latitude-longitude location. As
212 noted in section 2.3, both daily sonde and M2GMI TCO weare derived using the same NCEP
213 WMO tropopause pressures.

214

215 The M2GMI modelled ozone in Fig. 1 closely simulates the sonde measured ozone year-round
216 with an exception in the NH mid-high latitudes in MAM and JJA where the simulation tends to
217 underestimate sonde TCO by ~5 DU or more. Section S34 of the Supplementary Material
218 includes additional discussion and figures regarding evaluation of M2GMI tropospheric ozone
219 profiles using ozonesondes and surface lidar measurements.

220



221

222 **Figure 1.** Comparisons between M2GMI simulated (red curves) and ozonesonde TCO (blue
223 asterisks) averaged over three-month seasons (indicated) for 2004-2016. The M2GMI TCO field
224 is sampled daily at the sonde station locations. All TCO is in Dobson Units. The same daily
225 tropopause is used for both M2GMI and sonde to derive TCO, and is defined as according to the
226 WMO 2 K km^{-1} lapse-rate tropopause definition using NCEP temperatures. Included in each
227 panel are mean offsets and standard deviations of TCO seasonal differences.

228

229 **3. The MLS/GMI seasonal climatology.**

230

231 The MLS/GMI seasonal climatology product is derived for both volume mixing ratio (units
232 ppmv) and vertical column concentration (DU km^{-1}); the latter has vertical and latitudinal
233 structure that is closely similar to that of ozone number density and ozone partial pressure.
234 Standard deviations are reported for both mixing ratios and column concentrations based upon
235 all available daily ozone profiles over a given month and within every 5° latitude band. The
236 standard deviations provide a measure of climatological ozone variability and are important for
237 error covariance matrices included as a priori information in retrieval algorithms such as the
238 optimal estimation method of Rodgers (2000). We refer the reader to the Supplementary
239 Materials for further discussion and figures involving calculated standard deviations.

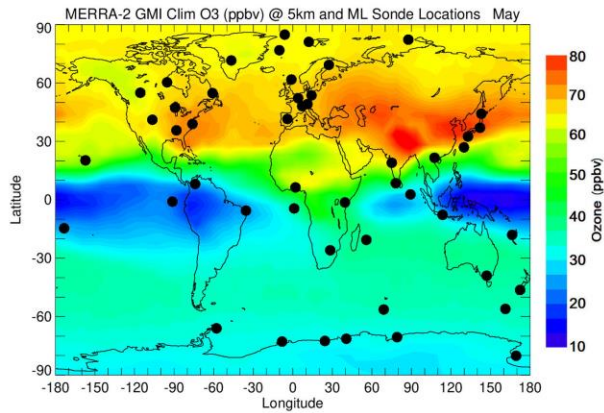
240

241 3.1. Global coverage of M2GMI tropospheric ozone compared to sondes.

242

243 Our motivation for using M2GMI simulation is that they provide better spatial and temporal
244 representation of tropospheric ozone profiles than ozonesondes. The sondes are sparsely
245 distributed over the Earth with generally only a few measured profiles per month for a given
246 station. The limited spatial coverage of sondes is demonstrated in Fig. 2 with M2GMI mid-
247 tropospheric ozone concentration (ppbv) at height $Z^* = 5$ km for climatological May (Z^* is
248 approximately equal to actual altitude and is defined in section 3.2.)

249



250

251 **Figure 2.** Map of climatological ozone volume mixing ratio (in ppbv) from the M2GMI
252 simulation at $Z^*=5$ km altitude (see section 3.2) for the month of May. Blue color indicates areas
253 with ozone concentration of about 10 ppbv and red color corresponds to regions with > 75 ppbv.
254 Black circles show locations of the sonde stations with a long observational record. Data from
255 these stations were used to constrain tropospheric ozone profiles in the ML climatology.

256

257 Tropospheric ozone exhibits planetary-scale variability that includes a year-round zonal wave-1
258 pattern in the tropics (greatest amplitude in September-October) and large-scale patterns outside
259 the tropics that vary greatly with season and region (Fishman et al., 1990). The tropical wave-1
260 in tropospheric ozone originates from regional sources of ozone: lightning, biofuel & biomass
261 burning, stratosphere-troposphere exchange (STE), and transport associated with the tropical
262 east-west Walker circulation. In the extra-tropics, the large planetary scale features in
263 tropospheric ozone have strong seasonal dependence with the seasonal maximum in JJA in the
264 NH and SON in the SH. These seasonal patterns in tropospheric ozone outside the tropics are
265 also due to combined effects from STE, biofuel, lightning, biomass burning, and long-range
266 transport. The global planetary-scale patterns in tropospheric ozone columns were first shown
267 from TOMS/SAGE (Fishman et al., 1990) and TOMS/MLS (Ziemke et al., 1996) satellite
268 measurements. The patterns in the M2GMI tropospheric ozone mixing ratio for $Z^* = 5$ km in
269 Fig. 2 in the tropics and in the NH are similar to the [TCO May pattern from satellite](#)
270 [records](#) ~~satellite TCO patterns during May.~~

271

272 It is apparent from Fig. 2 that the ensemble of ozonesondes is unlikely to effectively represent
273 the zonal mean tropospheric ozone values due to their limited sampling. For example, in the
274 tropics the sonde measurements under-sample the tropical wave-1 structure in tropospheric
275 ozone. Due to the under-sampling in the tropical Pacific area, sondes do not capture the very
276 low ozone concentrations of ~ 10 ppbv. This leads to the over-estimation of zonal-mean
277 tropospheric ozone in the tropics from the sondes. We will show later that this over-
278 determination of ML tropospheric ozone in the tropics averages to about 5-10 DU in TCO year-
279 round between 20°S - 20°N . The sondes also tend to miss the high values of ozone in the NH
280 mid-latitudes over the Asian continent (see Fig. 2), thus introducing a low bias in zonal-mean
281 tropospheric ozone in NH mid-latitudes.

282

283 3.2. Merging MLS and M2GMI ozone profiles.

284

285 Simulated ozone volume mixing ratio values from the M2GMI model were merged with ozone
286 volume mixing ratio measurements from MLS to construct ~~thean~~ ozone profile seasonal
287 climatology in the format of monthly zonal means. The merging of MLS and M2GMI ozone
288 involved monthly zonal-mean ozone profiles for both records in 5° latitude bands with Z*
289 altitudes 0-80 km (1 km increments). For low and mid-latitudes between 40°N and 40°S the
290 M2GMI and MLS profiles were merged for Z* levels between 13 km and 21 km (156 hPa to
291 49 hPa). For latitudes poleward of 40° in each hemisphere the profiles were merged slightly
292 lower in the atmosphere, for Z* levels between 8 km and 16 km (320 hPa to 101 hPa). Within
293 the merged altitude ranges the climatology is weighted linearly, from 100% M2GMI at the
294 lowest altitude to 100% MLS at the highest altitude. Standard deviations were calculated for
295 each climatological ozone value.

296

297 As in previous climatologies, the altitude variable used for our climatology is Z*, a parameter
298 frequently used in comparisons of atmospheric chemistry models (Park et al., 1999). Z* is in
299 units of kilometers but can be considered a pressure variable. Z*(km) is defined by
300 $Z^* = 16 \cdot \log(1013/P)$ where P is atmospheric pressure in units hPa. The altitude spacing for our
301 climatology is 1 km in Z* units. In an isothermal terrestrial atmosphere Z* would correspond
302 closely to altitude.

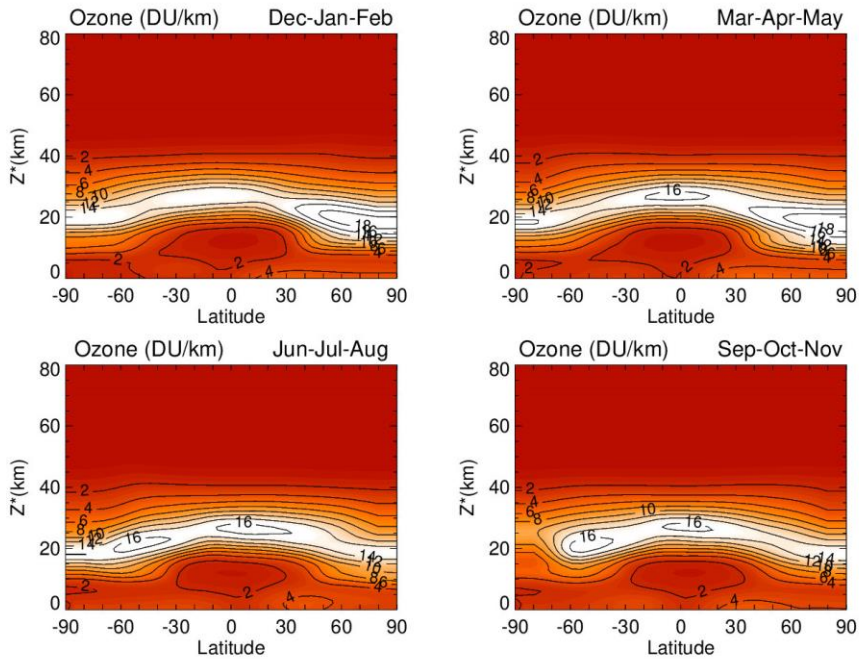
303

304 3.3. Comparisons with the ML Climatology.

305

306 We first examine basic global patterns of the MLS/GMI seasonal climatology. Figure 3 shows
307 vertical column concentrations (DU km⁻¹) for the climatology by 3-month season (indicated) for
308 Z* = 0-80 km. Column concentrations in the low stratosphere in both hemispheres are largest
309 during winter-spring and smallest in summer. In both hemispheres, ozone is largest in the
310 winter-spring months due to seasonal transport from the tropics to the extra-tropics in winter-
311 spring months (i.e., the Brewer Dobson Circulation) and longer lifetimes for ozone in the low
312 stratosphere. The highest ozone amounts in Fig. 3 are ~18-20 DU km⁻¹ in the NH around 20 km

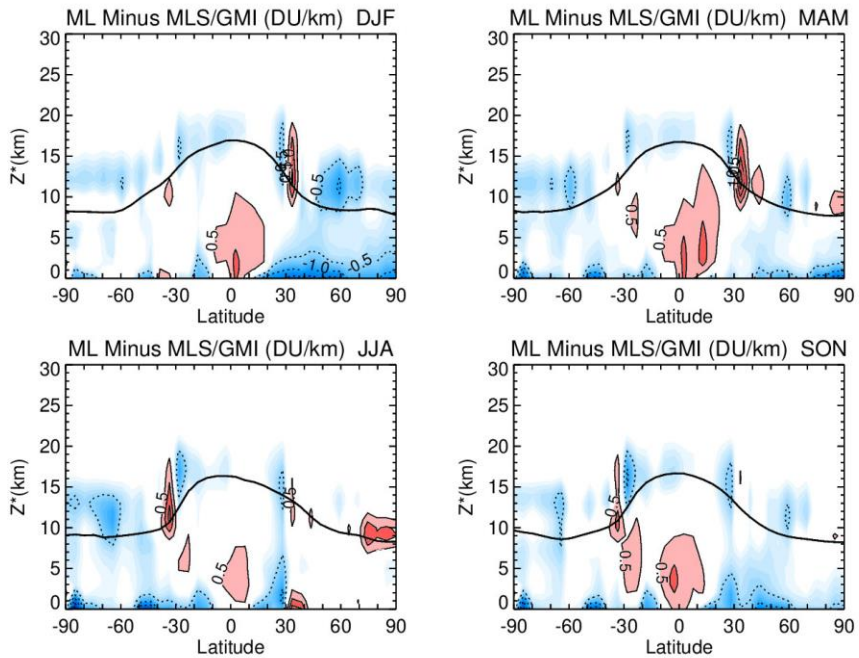
313 during winter and spring. In the troposphere, very low ozone density of less than 2 DU km⁻¹
314 occurs in the tropics year-round.
315



316
317 **Figure 3.** Meridional cross-sections of derived zonal-mean vertical ozone concentration (units
318 DU km⁻¹) for the MLS/GMI seasonal climatology. This 12-month climatology is averaged over
319 three-month seasons (indicated) for 2004-2016 and is binned for 5° latitude bands and Z* levels
320 from 0-80 km at 1 km spacing (see text).

321
322 While the basic characteristics of stratospheric ozone in Fig. 3 are important to note, our main
323 focus is to compare tropospheric ozone in Fig. 3 with the ML sonde ozone climatology. Because
324 the ML climatology uses sparsely sampled sonde measurements to estimate zonal-means in the
325 troposphere, it is possible that there may be substantial differences.
326

327 Figure 4 ~~shows the difference between ML and MLS/GMI~~ ~~compares MLS/GMI minus ML~~
328 zonal-mean ~~column profile~~ ozone by season, plotted as Z* altitude versus latitude. Only Z*
329 levels 0-30 km are included in Fig. 4 to highlight differences in ozone profiles used for the
330 troposphere and the low stratosphere merging region. Year-round positive differences in the
331 tropics in Fig. 4 suggest that ML is always too large in the low-mid troposphere compared to
332 M2GMI due to absence of ML sonde measurements in the Pacific region where tropospheric
333 ozone is low (e.g., Fig. 2). At latitudes around $\pm 35^\circ$ and elsewhere in the low stratosphere
334 merging region in Fig. 4 there are anomalous differences from -0.5 up to $+1.5$ DU km^{-1} ; these
335 sharp patterns are ascribed to sonde sampling issues for the ML climatology. In the boundary
336 layer throughout the NH extra-tropics during winter (i.e., upper left panel in Fig. 4) the M2GMI
337 ozone is higher than sondes by ~ 0.5 to 1 DU km^{-1} . These latter differences are attributed to a
338 known model issue related to underestimating surface deposition over cold surfaces (Jaegle et al.
339 2018), most prominent in the NH boundary layer during winter. When compared with ML in Fig.
340 4, the model ~~in this region~~ over-determines ~~the ozone column in DJF~~ by about 2 DU ~~in DJF~~.
341

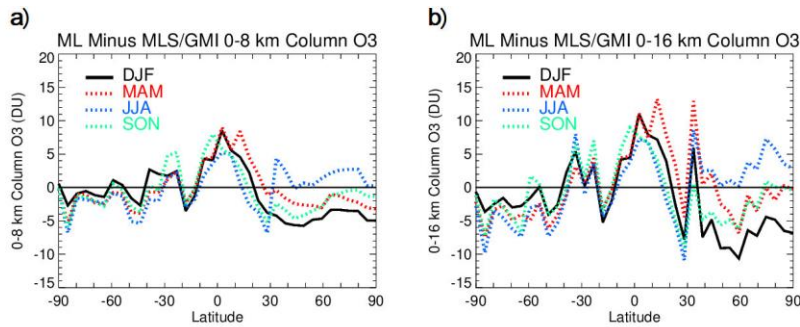


342
 343 **Figure 4.** Meridional cross-sections of ML minus MLS/GMI climatologies of ozone column
 344 concentration (DU km^{-1}). These differences are averaged over three-month seasons (indicated)
 345 for 2004-2016 and are binned for 10° latitude bands and Z^* levels from 0-30 km at 1 km spacing.
 346 Contour levels (indicated) increment by 0.5 DU km^{-1} with blue/dashed contours meaning
 347 negative, and pink/~~to~~ red solid contours meaning greater than 0.5 to 1.0 DU km^{-1} or greater. The
 348 black line indicates tropopause height according to the WMO 2 K km^{-1} lapse-rate tropopause
 349 definition using NCEP temperatures. White color denotes zero differences.

350
 351 Line plots of seasonal differences (ML minus MLS/GMI) of integrated ozone columns are
 352 shown in Fig. 5 for 0-8 km (Fig. 5a) and 0-16 km (Fig. 5b). These line plots are determined from
 353 Fig. 4 by summing the 1 km layers of ML minus MLS/GMI differences. In the tropics 0-16 km
 354 integrated column in Fig. 5b represents the total troposphere (i.e., TCO) with ML larger than
 355 MLS/GMI by about 10 DU year-round. Comparison with the 0-8 km columns in the left panel
 356 show that these differences in the tropics originate mostly from the lower troposphere which is

357 consistent with all four panels in Fig. 4. Outside the tropics in Fig. 5 there are seasonal offset
 358 differences in the NH up to -5 to -10 DU during DJF. Part of the reason for the ML minus
 359 MLS/GMI ~~seasonal~~ biases in Fig. 5 is due to sonde under-sampling for the ML climatology,
 360 particularly in the tropics as noted for Fig. 4. The sonde under-sampling also creates the sharp
 361 (non-physical) variability seen between adjacent latitude bins in Fig. 5.

362



363

364 **Figure 5.** (a) Line plots of seasonal differences of ML minus MLS/GMI integrated ozone
 365 columns for 0-8 km. The differences are averaged over three-month seasons (indicated by DJF,
 366 MAM, JJA, and SON). (b) Same as (a), but for 0-16 km ozone columns.

367

368 4. An inter-annual ozone profile climatology.

369

370 The MLS/GMI seasonal climatology captures the ~~mean~~-vertical shape of zonal-mean ozone
 371 profiles by season and latitude in both troposphere and stratosphere. However, inter-annual
 372 processes such as the QBO produce sizeable changes in the vertical ozone distribution in
 373 stratospheric ozone from year to year. To capture these variations, we have constructed a global
 374 time-dependent climatology of stratospheric ozone that represents ozone inter-annual variability.
 375 This climatology can be used either independently or added to the MLS/GMI seasonal
 376 climatology, depending on the particular application.

377

378 The derivation of the inter-annual ozone climatology is lengthy and is discussed in detail in the
 379 Supplementary Materials. In this section we provide only a short overview of the methodology
 380 and discuss the final product. The inter-annual ozone climatology is constructed using a method

381 that includes an REOF analysis as described by Richman (1986, and references therein). With
382 our approach, vertical information ~~for the climatology is derived~~ comes from an REOF analysis
383 of MLS ozone profiles, while ~~month-to-month~~ time dependence ~~follows is provided~~ by coupling
384 the REOF analysis time coefficients with SBUV MOD total ozone and tropical QBO zonal
385 winds. The time period for the REOF climatology depends on the availability of total ozone and
386 tropical QBO winds. The time period for this climatology is 1970-2018 (~~588 consecutive~~
387 ~~months~~) with gaps present due to some missing MOD total ozone including Nimbus 4
388 measurements in the 1970s. We plan to periodically extend this REOF climatology when zonal
389 wind and MOD total ozone data become available.

390
391 ~~We demonstrate that the REOF climatology does very well in capturing inter-annual variability~~
392 ~~of stratospheric ozone. The excellent vertical resolution of MLS ozone limb measurements of ~3~~
393 ~~km resolves much of the vertical variability of ozone caused by low-frequency and episodic~~
394 ~~processes such as the QBO, extra-tropical stratospheric warmings, and year-round planetary-~~
395 ~~scale wave events (e.g., Ziemke et al., 2014, and references therein). Many nadir instrument~~
396 ~~ozone profile retrievals have coarse vertical resolution of ~10 km or greater (such as from SBUV~~
397 ~~or OMI) and cannot do nearly as well at resolving vertical changes in stratospheric ozone.~~

398
399 ~~We provide a short description of the REOF method and refer to the Supplementary Materials~~
400 ~~for details regarding the calculations. Before applying the REOF approach, an~~ The Empirical
401 Orthogonal Function (EOF) method (Kutzbach 1967, and references therein) was applied to
402 MLS ozone anomaly profiles to derive repeatable inter-annual patterns in the ozone vertical
403 distribution; ~~that is, (~~ The EOF analysis was applied to MLS monthly zonal-mean ozone profile
404 anomalies derived by removing seasonal cycles ~~in MLS monthly zonal-mean profiles~~ between
405 ~~August/January~~ 2004~~5~~ and December 2016. All MLS ozone and anomaly ozone p Profiles were
406 binned into 5° latitude bands (36 bands for 90°S-90°N, similar to MLS/GMI climatology)
407 between 1 and 261 hPa (30 pressure levels).

408
409 The main challenge of EOF analysis is interpretation of derived EOFs and EOF time
410 coefficients and their attribution to specific geophysical processes. ~~As described in the~~
411 Supplementary Materials, the construction of this REOF climatology required only total ozone

412 ~~and tropical stratospheric zonal wind time series in the stratosphere to explain most of~~
413 ~~stratospheric ozone profiles variability (total EOF variance). In this study we applied rotated~~
414 ~~EOFs which helped us to attribute our EOF results to specific geophysical quantities, that is, total~~
415 ~~column ozone and equatorial zonal wind. The step by step methodology for developing the~~
416 ~~REOF-based inter-annual ozone profile anomaly climatology is described in the Supplementary~~
417 ~~Materials.~~ We used MLS ozone anomalies expressed as ozone partial pressure for the REOF
418 analysis rather than ozone mixing ratio because it helped to attribute the REOF-1 time coefficient
419 directly to total ozone column measurements at all latitudes. The first REOF vector with the
420 MOD SBUV total ozone time series as a proxy explains about 50-70% of the inter-annual ozone
421 variability. Next, we derived a second REOF (REOF-2) that we attributed to the QBO and used
422 the equatorial zonal wind time series as a proxy for REOF-2. The sum of these two REOFs
423 explains about 70-80% of the inter-annual variability in de-seasonalized MLS zonal mean ozone
424 profiles. Since only MLS profiles are used to constrain the vertical shapes of the REOFs and
425 time coefficients are described by total ozone and zonal winds, this REOF climatology can be
426 used in the future (even after MLS stops operating) or can be extended into the past to the pre-
427 Aura time period whenever total column ozone and wind data are available.

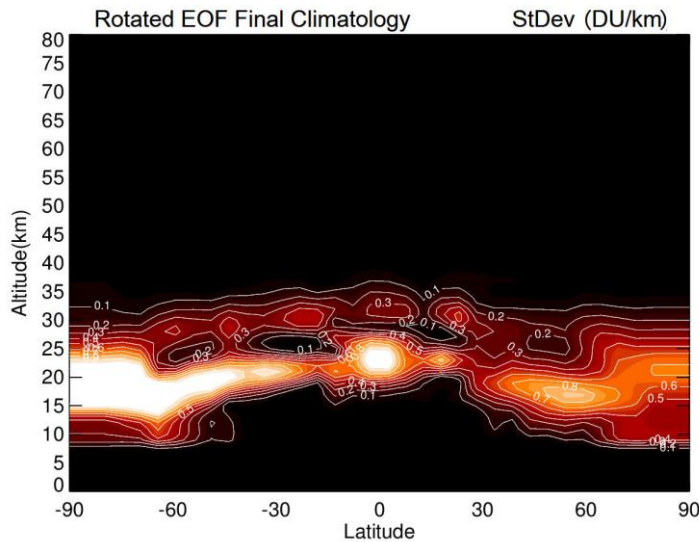
428
429 The REOF climatology was finally converted from the ozone partial pressures defined at 30
430 MLS levels to volume mixing ratio (ppmv) and partial ozone column (DU km^{-1}) at the 1 km Z^*
431 levels (defined in section 3.2) identical to the MLS/GMI climatology. The REOF climatological
432 values at levels below ~9 km and above ~48 km are very small in contributing to inter-annual
433 variability of ozone and are set to zero. Since the REOF climatology uses zonal wind and total
434 ozone time series that can have long-term trends, we applied a very low frequency (VLF) digital
435 low-pass filter to the final derived REOF climatology to remove long-term decadal variability.
436 This was done to ensure that the climatology captures only inter-annual variability in monthly
437 zonal mean ozone anomaly profiles without inducing decadal trends if used as a prior in ozone
438 retrieval. The frequency response of the applied VLF digital filter (Stanford and Ziemke, 1993)
439 is exactly 0.0 (1.0) at zero (Nyquist) frequency with an amplitude of 0.5 at frequency 0.00333
440 month^{-1} ; the filter was also designed to have zero phase shift at all frequencies.

441

442 We demonstrate that the REOF climatology does very well in capturing inter-annual variability
443 of monthly zonal-mean stratospheric ozone. The excellent^{high} vertical resolution of MLS ozone
444 limb measurements of ~3 km resolves much of the vertical variability of ozone caused by low-
445 frequency and episodic processes such as the QBO, extra-tropical stratospheric warmings, and
446 other year-round planetary-scale wave events (e.g., Ziemke et al., 2014, and references therein).
447 Many nadir instrument ozone profile retrievals have coarse vertical resolution of ~ 6 to ~10 km
448 or greater (such as from SBUV or OMI) and cannot do nearly as well at resolving vertical
449 changes in stratospheric ozone.

450
451 The magnitude of inter-annual variability in profile ozone, captured by the REOF climatology, is
452 shown in Fig. 6 as calculated standard deviations in DU km⁻¹ for the 1970-2018 period. In the
453 tropical low latitudes from 10°S-10°N the main source of inter-annual variability is the QBO.
454 However, larger inter-annual variability occurs in the SH extra-tropics due to the QBO and
455 additional dynamical sources. In an effort to understand the contribution of non-QBO processes
456 to the inter-annual variability we also generated a climatology ~~based on~~ using only equatorial
457 QBO zonal winds as a proxy (see Fig. S4 in the Supplementary Material). When compared to
458 the REOF climatology in Fig. 6, only a very small fraction of inter-annual variability is captured
459 in the extra-tropics for the QBO-only climatology.

460



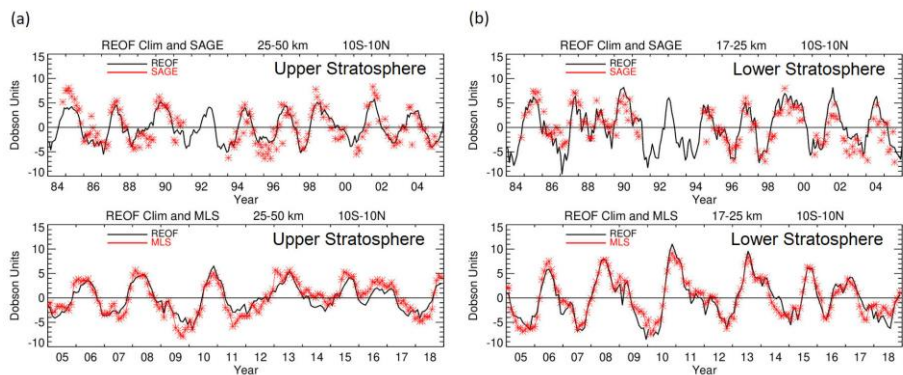
461
 462 **Figure 6.** Temporal standard deviation (in DU km^{-1}) for 1970-2018 for the final REOF ozone
 463 climatology (i.e., Eq. (S10) in Supplementary Materials). The inter-annual variability in the
 464 tropical low latitudes is almost entirely due to the QBO. Inter-annual variability in the extra-
 465 tropics comes from the QBO coupled with other non-QBO related inter-annual variability.

466
 467 The long record of the REOF inter-annual ozone profile climatology has been compared with de-
 468 seasonalized ozone profile measurements from SAGE II and Aura MLS for 1984-2018 (Fig. 7).
 469 The top panel in Fig. 7a shows comparisons of upper stratospheric column ozone anomalies
 470 ($Z^* = 25\text{-}50$ km) between REOF (black curve) and SAGE (red asterisks) for years 1984-2005 in
 471 the tropics ($10^\circ\text{S}\text{-}10^\circ\text{N}$). The bottom panel in Fig. 7**ab** shows a similar comparison between
 472 REOF and MLS for 2005-2018. Figure 7b is the same as in Fig. 7a, except for the lower
 473 stratosphere ($Z^* = 17\text{-}25$ km).

474
 475 The SAGE II sampling ozone columns in Fig. 7 is sparse, averaging $\sim 2\text{-}3$ days of measurements
 476 for a given month in the $10^\circ\text{S}\text{-}10^\circ\text{N}$ latitude band shown. This means that the monthly SAGE
 477 measurements in Fig. 7 are more representative of daily profiles rather than monthly means.
 478 Ozone profiles on a daily basis in the tropics are distorted by propagating tropical waves with

479 periods of days to weeks such as Kelvin waves, equatorial Rossby waves, and mixed Rossby-
 480 gravity waves (e.g., Timmermans et al., 2005; Ziemke and Stanford, 1994). As a result, the
 481 upper and lower stratospheric columns in Fig. 7 for SAGE II will have noisy month-to-month
 482 variations of several DU because of these tropical waves. The Supplementary Material includes
 483 further discussion and figures for the REOF climatology.

484



485

486 **Figure 7.** (a) Top panel is zonal-mean upper stratospheric column ozone (in Dobson Units) for
 487 the REOF climatology (black curve) and deseasonalized SAGE II (red asterisks) spanning 1984-
 488 2005 and averaged between 10°S-10°N. The SAGE data are deseasonalized monthly zonal
 489 means. All column amounts are calculated by integrating ozone profiles for Z^* =25-50 km (~28
 490 to 1 hPa). Bottom panel is the same as the top panel, but with MLS in place of SAGE and for the
 491 time period 2005-2018. (b) Same as (a), but for the lower stratosphere with Z^* =17-25 km (~88
 492 to 28 hPa).

493

494 **5. Summary.**

495

496 We have produced a new MLS/GMI seasonal ozone profile climatology by combining ozone
 497 profiles from the M2GMI model simulation with MLS v4.2 measurements. M2GMI is used
 498 primarily for tropospheric ozone and MLS for stratospheric ozone, with the two ozone profile
 499 datasets blended together in the low stratosphere; the result is a merged zonal-mean, 12-month
 500 global ozone profile climatology at 5° latitude resolution with Z^* altitude range 0-80 km (1 km

501 vertical sampling). Our main interest in generating the MLS/GMI climatology is to use it as a
502 priori information in satellite ozone retrieval algorithms. However, it is also useful as a baseline
503 for evaluating various modeled or measured ozone [seasonal and inter-annual variability](#), and in
504 studies involving [corresponding ozone radiative forcing as inferred from](#) atmospheric radiative
505 transfer calculations.

506

507 In previous studies we generated several ozone profile climatologies based on combining
508 ozonesondes with either SAGE or MLS satellite measurements (e.g., McPeters et al., 2007;
509 McPeters and Labow, 2012; Labow et al., 2015). We have compared the new MLS/GMI
510 climatology in detail with the ML climatology of McPeters and Labow (2012) that used
511 ozonesondes for tropospheric ozone profiles. The M2GMI model simulation provides an
512 improved ozone climatology for the troposphere compared to the ML climatology due to having
513 much better spatial and temporal coverage than the sondes.

514

515 We also developed a time-dependent climatology of monthly zonal-mean profile ozone
516 anomalies representing inter-annual variability. This inter-annual climatology was constructed
517 using a rotational EOF analysis of Aura MLS monthly zonal-mean profile ozone anomalies from
518 August 2004 – December 2016 within each 5° latitude band. The analysis shows that the first
519 two leading EOFs explain ~70-80% of inter-annual variability of profile ozone at all latitudes.
520 Furthermore, total ozone and tropical zonal wind time series correlate well with the two leading
521 EOF coefficient time series and were used as proxies to extend information outside the Aura
522 MLS time range. We used these relationships to reconstruct anomalies at 5° latitudinal resolution
523 for $Z^* = 0-80$ km and 1970-2018. This REOF time-dependent climatology was compared to a
524 similar climatology based on only tropical QBO winds. The advantage of the REOF climatology
525 is that allows for a much more thorough representation of inter-annual variability of stratospheric
526 ozone than just the QBO.

527

528 The REOF time-dependent climatology of ozone profile anomalies can be easily added to the
529 MLS/GMI seasonal climatology to simulate seasonal+inter-annual variability of stratospheric
530 ozone. We note that both the MLS/GMI 12-month climatology and REOF climatology were

531 generated using Aura time period MLS ozone measurements and neither of them account for
532 long-term trends in stratospheric ozone.

533

534

535 **Acknowledgments.** We thank the NASA Jet Propulsion Laboratory MLS team for the MLS
536 v4.2 ozone dataset and the SHADOZ, WOUDC and NDACC personnel for providing the
537 extensive ozonesonde measurements that we used for our study. We also thank the NASA MAP
538 program for supporting the MERRA-2 GMI simulation and the NASA Center for Climate
539 Simulation (NCCS) for providing high-performance computing resources. Special thanks go to
540 the NASA GMI group especially Sarah Strode regarding the MERRA-2 GMI simulation.

541 Funding for this research was provided in part by NASA NNN14ZDA001N-DSCOVER.

542

543

544 **Data availability.** Data description for MLS v4.2 ozone and links to the data can be obtained
545 from websites https://mls.jpl.nasa.gov/products/o3_product.php (last access 16 April 2021) and
546 <https://disc.gsfc.nasa.gov/> (last access 16 April 2021). MERRA-2 GMI model description and
547 access is available at <https://acd-ext.gsfc.nasa.gov/Projects/GEOSCCM/MERRA2GMI/> (last
548 access: 16 April 2021). The MOD total ozone measurements are available from the webpage
549 https://acd-ext.gsfc.nasa.gov/Data_services/merged/. Tropical QBO winds were provided by the
550 University of Berlin from <https://www.geo.fu-berlin.de/met/ag/strat/produkte/qbo/qbo.dat>. The
551 seasonal and inter-annual climatology products derived from our study are available for the
552 general public using direct links from the NASA webpage <https://avdc.gsfc.nasa.gov/>.

553

554

555 **References.**

556

557 Bass, A. M., and R. J. Paur, The ultraviolet cross-sections of ozone, I: The measurements, in
558 *Proc. Quad. Ozone Symp.*, edited by C. Zerefos, and A. Ghazi, pp. 606–616, Reidel, Dordrecht,
559 Halkidiki, Greece, 1984.

560

561 Bourgeois, I., J. Peischl, C. R. Thompson, K. C. Aikin, T. Campos, H. Clark, R. Commane, B.
562 Daube, G. W. Diskin, J. W. Elkins, R.-S. Gao, A. Gaudel, E. J. Hints, B. J. Johnson, R. Kivi, K.
563 McKain, F. L. Moore, D. D. Parrish, R. Querel, E. Ray, R. Sánchez, C. Sweeney, D. W.
564 Tarasick, A. M. Thompson, V. Thouret, J. C. Witte, S. C. Wofsy, and T. B. Ryerson, Global-scale
565 distribution of ozone in the remote troposphere from the ATom and HIPPO airborne field
566 missions *Atmos. Chem. Phys.*, 20, 10611–10635, <https://doi.org/10.5194/acp-20-10611-2020>,
567 2020.

568

569 Duncan, B. N., R. V. Martin, A. C. Staudt, R. Yevich, and J. A. Logan, Interannual and seasonal
570 variability of biomass burning emissions constrained by satellite observations, *J. Geophys. Res.*
571 *Atmos.*, 108(D2), doi:10.1029/2002jd002378, 2003.

572

573 Duncan, B.N., S.E. Strahan, Y. Yoshida, S.D. Steenrod, and N. Livesey, Model study of cross-
574 tropopause transport of biomass burning pollution, *Atmos. Chem. Phys.*, 7, 3713-3736,
575 doi:10.5194/acp-7-3713-2007, 2007.

576

577 Fishman, J., C. E. Watson, J. C. Larsen, and J. A. Logan, Distribution of tropospheric ozone
578 determined from satellite data, *J. Geophys. Res.*, 95(D4), 3599-3617, 1990.

579

580 Frith, S. M., N. A. Kramarova, R. S. Stolarski, R. D. McPeters, P. K. Bhartia, and G. J. Labow,
581 Recent changes in total column ozone based on the SBUV Version 8.6 Merged Ozone Data Set,
582 *J. Geophys. Res. Atmos.*, 119, 9735–9751, doi:10.1002/2014JD021889, 2014.

583

584 Frith, S. M., P. K. Bhartia, L. D. Oman, N. A. Kramarova, R. D. McPeters, and G. J. Labow,
585 Model-based climatology of diurnal variability in stratospheric ozone as a data analysis tool
586 *Atmos. Meas. Tech.*, 13, 2733–2749, <https://doi.org/10.5194/amt-13-2733-2020>, 2020.

587

588 Froidevaux, L., et al., Validation of Aura Microwave Limb Sounder stratospheric ozone
589 measurements, *J. Geophys. Res.*, 113, D15S20, doi:10.1029/2007JD008771, 2008.

590

591 Gelaro, R., W. McCarty, M.J. Suárez, R. Todling, A. Molod, L. Takacs, C.A. Randles, A.
592 Darnenov, M.G. Bosilovich, R. Reichle, K. Wargan, L. Coy, R. Cullather, C. Draper, S. Akella,
593 V. Buchard, A. Conaty, A.M. da Silva, W. Gu, G. Kim, R. Koster, R. Lucchesi, D. Merkova, J.E.
594 Nielsen, G. Partyka, S. Pawson, W. Putman, M. Rienecker, S.D. Schubert, M. Sienkiewicz, and
595 B. Zhao, The Modern-Era Retrospective Analysis for Research and Applications, Version 2
596 (MERRA-2), *J. Climate*, 30, 5419–5454, <https://doi.org/10.1175/JCLI-D-16-0758.1>, 2017.
597
598 Giglio, L., J. Randerson, and G. van der Werf, Analysis of daily, monthly, and annual burned
599 area using the fourth-generation global fire emissions database (GFED4), *J. Geophys. Res.*
600 *Bio.Sci.*, 118(1), 317-328, doi:10.1002/jgrg.20042, 2013.
601
602 Granier, C., B. Bessagnet, T. Bond, A. D'Angiola, H. D. van der Gon, et al., Evolution of
603 anthropogenic and biomass burning emissions of air pollutants at global and regional scales
604 during the 1980–2010 period. *Climatic Change*, 109, 163–190, doi:10.1007/s10584-011-0154-1,
605 2011.
606
607 Jaeglé, L., V. Shah, J. A. Thornton, F. D. Lopez-Hilfiker, B. H. Lee, E. E. McDuffie, et al.,
608 Nitrogen oxides emissions, chemistry, deposition, and export over the Northeast United States
609 during the WINTER aircraft campaign, *J. Geophys. Res. Atmos.*, 123, 12,368–12,393,
610 <https://doi.org/10.1029/2018JD029133/>, 2018.
611
612 Jiang, Y. B., et al., Validation of Aura Microwave Limb Sounder Ozone by ozonesonde and lidar
613 measurements, *J. Geophys. Res.*, 112, D24S34, doi:10.1029/2007JD008776, 2007.
614
615 Kutzbach, J. E., Empirical eigenvectors of sea-level pressure, surface temperature and
616 precipitation complexes over North America, *J. App. Meteorol.*, 6, 791-802,
617 [https://doi.org/10.1175/1520-0450\(1967\)006<0791:EEOSLP>2.0.CO;2](https://doi.org/10.1175/1520-0450(1967)006<0791:EEOSLP>2.0.CO;2), 1967.
618

619 Labow, G. J., J. R. Ziemke, R. D. McPeters, D. P. Haffner, and P. K. Bhartia, A total ozone-
620 dependent ozone profile climatology based on ozonesondes and Aura MLS data, *J. Geophys.*
621 *Res. Atmos.*, *120*, 2537-2545, doi:10.1002/2014JD022634, 2015.

622

623 Lamarque, J.-F., T. C. Bond, V. Eyring, C. Granier, A. Heil, Z. Klimont, D. Lee, C. Liousse, A.
624 Mieville, B. Owen, M. G. Schultz, D. Shindell, S. J. Smith, E. Stehfest, J. Van Aardenne, O. R.
625 Cooper, M. Kainuma, N. Mahowald, J. R. McConnell, V. Naik, K. Riahi, and D. P. van Vuuren,
626 Historical (1850-2000) gridded anthropogenic and biomass burning emissions of reactive gases
627 and aerosols: methodology and application, *Atmos. Chem. Phys.*, *10*(15), 7017-7039,
628 doi:10.5194/acp-10-7017-2010, 2010.

629

630 Livesey, N. J., Read, W. G., Froidevaux, L., Lambert, A., Manney, G. L., Pumphrey, H. C.,
631 Santee, M. L., Schwartz, M. J., Wang, S., Cofield, R. E., Cuddy, D. T., Fuller, R. A., Jarnot, R.
632 F., Jiang, J. H., Knosp, B. W., Stek, P. C., Wagner, P. A., and Wu, D. L.: *EOS MLS Version 3.3*
633 *Level 2 data quality and description document, Tech. rep., Jet Propulsion Laboratory*, available
634 at: <http://mls.jpl.nasa.gov/>, 2011.

635

636 McPeters, R. D., G. J. Labow, and J. A. Logan, Ozone climatological profiles for satellite
637 retrieval algorithms, *J. Geophys. Res.*, *112*, D05308, doi:10.1029/2005JD006823, 2007.

638

639 McPeters, R. D., and G. J. Labow, Climatology 2012: An MLS and sonde derived ozone
640 climatology for satellite retrieval algorithms, *J. Geophys. Res.*, *117*, doi:10.1029/2011JD017006,
641 2012.

642

643 McPeters, R. D., P. K. Bhartia, D. Haffner, G. J. Labow, and L. Flynn, The version 8.6 SBUV
644 ozone data record: An overview, *J. Geophys. Res.*, *118*, 8032–8039, doi:10.1002/jgrd.50597,
645 2013.

646

647 Molod, A., L. Takacs, M. Suarez, and J. Bacmeister, Development of the GEOS-5 atmospheric
648 general circulation model: evolution from MERRA to MERRA2, *Geosci. Mod. Dev.*, *8*,
649 doi:10.5194/gmd-8-1339-2015, 2015.

650
651 Oman, L. D., A. R. Douglass, J. R. Ziemke, J. M. Rodriguez, D. W. Waugh, and J. E. Nielsen,
652 The ozone response to ENSO in Aura satellite measurements and a chemistry-climate
653 simulation, *J. Geophys. Res.*, *118*, 965-976, doi:10.1029/2012JD018546, 2013.
654
655 Orbe, C., L. D. Oman, S. E. Strahan, D. W. Waugh, S. Pawson, L. L. Takacs, and A. M. Molod,
656 Large-Scale Atmospheric Transport in GEOS Replay Simulations, *J. Adv. Mod. Earth Sys.*, *9*,
657 2545-2560, 2017.
658
659 Park, J. H., M. K. Ko, C. H. Jackman, R. A. Plumb, J. A. Kaye, and K. H. Sage, Models and
660 Measurements Intercomparison II, *NASA Tech. Memo.*, *NASA/TM-1999-209554*, 502 pp., 1999.
661
662 Parrish, A., Boyd, I. S., Nedoluha, G. E., Bhartia, P. K., Frith, S. M., Kramarova, N. A., Connor,
663 B. J., Bodeker, G. E., Froidevaux, L., Shiotani, M., and Sakazaki, T.: Diurnal variations of strato-
664 spheric ozone measured by ground-based microwave remote sensing at the Mauna Loa NDACC
665 site: measurement validation and GEOSCCM model comparison, *Atmos. Chem. Phys.*, *14*, 7255-
666 7272, <https://doi.org/10.5194/acp-14-7255-2014>, 2014.
667
668 Richman, M. B., Rotation of principal components, *J. Clim.*, *6*, 293-335,
669 <https://doi.org/10.1002/joc.3370060305>, 1986.
670
671 Rodgers, C. D., Inverse methods for atmospheric sounding: theory and practice, *World Scientific*
672 *Publishing Co.*, pp. 238, London, United Kingdom, 2000.
673
674 Shepherd, T. G., D. A. Plummer, J. F. Scinocca, M. I. Hegglin, V. E. Fioletov, M. C. Reader, E.
675 Remsberg, T. von Clarmann, and H. J. Wang, Reconciliation of halogen-induced ozone loss with
676 the total-column ozone record, *Nature Geosci.*, *7*, doi:10.1038/NGEO2155, 2014.
677
678 Stanford, J. L., J. R. Ziemke, and S. Y. Gao, Stratospheric circulation features deduced from
679 SAMS constituent data, *J. Atmos. Sci.*, *50*, 226-246, 1993.
680

681 Stauffer, R. M., A. M. Thompson, L.D. Oman, and S.E. Strahan, The effects of a 1998 observing
682 system change on MERRA-2-based ozone profile simulations. *J. Geophys. Res. Atmos.*, 124,
683 7429-7441, <https://doi.org/10.1029/2019JD030257>, 2019.

684

685 Strode, S. A., J. M. Rodriguez, J. A. Logan, O. R. Cooper, J. C. Witte, L. N. Lamsal, M. Damon,
686 B. Van Aartsen, S. D. Steenrod, and S. E. Strahan, Trends and variability in surface ozone over
687 the United States, *J. Geophys. Res. Atmos.*, 120(17), 9020-9042, doi:10.1002/2014JD022784,
688 2015.

689

690 Strode, S. A., J. S. Wang, M. Manyin, B. N. Duncan, R. Hossain, C. A. Keller, S. E. Michel, and
691 J. W. C. White, Strong sensitivity of the isotopic composition of methane to the plausible range
692 of tropospheric chlorine, *Atmos. Chem. Phys.*, 20, 8405–8419, [https://doi.org/10.5194/acp-20-](https://doi.org/10.5194/acp-20-8405-2020)
693 [8405-2020](https://doi.org/10.5194/acp-20-8405-2020), 2020.

694

695 Thompson, A. M., Witte, J. C., Sterling, C., Jordan, A., Johnson, B. J., Oltmans, S. J., Fujiwara,
696 M., Vömel, H., Allaart, M., Peters, A., Coetzee, G. J. R., Posny, F., Corrales, E., Andres Diaz, J.,
697 Félix, C., Komala, N., Lai, N., Maata, M., Mani, F., Zainal, Z., Ogino, S.-Y., Paredes, F., Luiz
698 Bezerra Penha, T., Raimundo da Silva, F., Sallons-Mitro, S., Selkirk, H. B., Schmidlin, F. J.,
699 Stuebi, R., and Thiongo, K.: First reprocessing of Southern Hemisphere Additional Ozonesondes
700 (SHADOZ) Ozone Profiles (1998–2016). 2. Comparisons with satellites and ground-based
701 instruments, *J. Geophys. Res.*, 122, 13000–13025, <https://doi.org/10.1002/2017JD027406>, 2017.

702

703 Timmermans, R. M. A., R. F. van Oss, and H. M. Kelder, Equatorial Kelvin wave signatures in
704 ozone profile measurements from Global Ozone Monitoring Experiment (GOME), *J. Geophys.*
705 *Res.*, 110, D21103, doi:10.1029/2005JD005929, 2005.

706

707 Wallace, J. M., R. L. Panetta, and J. Estberg, Representation of the equatorial stratospheric
708 Quasi-Biennial Oscillation in EOF phase space, *J. Atmos. Sci.*, 50, 12, 1751-1762,
709 doi:10.1175/1520-0469(1993)050<1751:ROTESQ>2.0.CO;2, 1993.

710

711 Wargan, K., C. Orbe, S. Pawson, J. R. Ziemke, L. D. Oman, M. A. Olsen, et al., Recent decline
712 in extratropical lower stratospheric ozone attributed to circulation changes. *Geophys. Res. Lett.*,
713 *45*, 5166–5176. [https:// doi.org/10.1029/2018GL077406](https://doi.org/10.1029/2018GL077406), 2018.

714

715 Witte, J. C., Thompson, A. M., Smit, H. G. J., Fujiwara, M., Posny, F., Coetzee, G. J. R.,
716 Northam, E. T., Johnson, B. J., Sterling, C. W., Mohammed, M., Ogino, S.-Y., Jordan, A.,
717 daSilva, F. R., and Zainal, Z.: First reprocessing of Southern Hemisphere Additional
718 OZonesondes (SHADOZ) profile records (1998–2015) 1: Methodology and evaluation, *J.*
719 *Geophys. Res.*, *122*, 6611–6636, <https://doi.org/10.1002/2016JD026403>, 2017.

720

721 Ziemke, J. R., and J. L. Stanford, Quasi-biennial oscillation and tropical waves in total ozone, *J.*
722 *Geophys. Res.*, *99*, 23,041-23,056, 1994.

723 Ziemke, J. R., S. Chandra, A. Thompson, and D. McNamara, Zonal asymmetries in Southern
724 Hemisphere column ozone: Implications of biomass burning, *J. Geophys. Res.*, *101*, 14,421-
725 14,427, doi:10.1029/96JD01057, 1996.

726 Ziemke, J. R., S. Chandra, G. J. Labow, P. K. Bhartia, L. Froidevaux, and J. C. Witte, A global
727 climatology of tropospheric and stratospheric ozone derived from Aura OMI and MLS
728 measurements, *Atmos. Chem. Phys.*, *11*, 9237-9251, doi:10.5194/acp-11-9237-2011, 2011.

729

730 Ziemke, J. R., M. A. Olsen, J. C. Witte, A. R. Douglass, S. E. Strahan, K. Wargan, X. Liu, M. R.
731 Schoeberl, K Yang, T. B. Kaplan, S. Pawson, B. N. Duncan, P. A. Newman, P. K. Bhartia, M. K.
732 Heney, Assessment and applications of NASA ozone data products derived from Aura
733 OMI/MLS satellite measurements in context of the GMI Chemical Transport Model, *J. Geophys.*
734 *Res. Atmos.*, *119*, 5671-5699,doi:10.1002/2013JD020914, 2014.

735